IEEE Access
Multidisciplinary ⋮ Rapid Review ⋮ Open Access Journal

Received 21 January 2024, accepted 13 February 2024, date of publication 21 February 2024, date of current version 29 February 2024.

Digital Object Identifier 10.1109/ACCESS.2024.3368861

RESEARCH ARTICLE

Meta-Heuristics Based Design and Optimization of Active Clamp Flyback Converter for USB PD

OMER SAID AYDIN[1], ABDULSAMED LORDOGLU[1,2,3], (Member, IEEE), MELTEM LORDOGLU[1], ARDA AKYILDIZ[1], BATI EREN ERGUN[1,2], AND MEHMET ONUR GULBAHCE[1,2], (Member, IEEE)

[1]Department of Electrical Engineering, Istanbul Technical University, 34469 İstanbul, Turkey
[2]ITU Advanced Vehicle Technologies Application and Research Center, ILATAM, 34485 İstanbul, Turkey
[3]Energy Institute, Istanbul Technical University, 34469 İstanbul, Turkey

Corresponding author: Mehmet Onur Gulbahce (ogulbahce@itu.edu.tr)

This work was supported by Istanbul Technical University (ITU) Scientific Research Projects Unit (BAP) under Project MYL-2022-43630 and Project MGA-2022-43948.

ABSTRACT The escalating demand for small, compact, and economical consumer electronics necessitates efficient power conversion at higher switching frequencies. The active-clamp flyback (ACF) converter, offering isolation, efficient performance at low and medium power levels, and cost and volume efficiency, is frequently employed in consumer electronics, including USB PD devices. However, designing and selecting components for the ACF converter remains a challenging task, particularly for fast charging and USB-PD standards. This paper introduces a comprehensive design and optimization methodology for the ACF converter under constraints of power loss, volume, and efficiency. This methodology employs the particle swarm optimization algorithm, a nature-inspired optimization technique. The proposed design and optimization algorithm provides a detailed design process and aids designers in determining the optimal size of the ACF converter. The optimization algorithm orchestrates the circuit design by selecting design parameters within a certain frequency range, utilizing transformer, switches, and diode elements from the database. In consideration of the requirement for high-frequency operation, the database also includes GaN semiconductor switches and high-frequency operated magnetic components. The design presenting the highest benefits in terms of volume, cost, and losses is selected using the converter level fitness function, which incorporates cost, volume, and loss considerations. To evaluate the proposed design and optimization methodology, a USB PD converter capable of providing 5V/9V/15V/20V DC voltages (max. 65W) from a 230 VAC/50 Hz supply was designed and its performance analyzed.

INDEX TERMS Active clamp, active clamp flyback circuit, nature-inspired optimization techniques, particle swarm optimization, synchronous rectifier, USB PD.

I. INTRODUCTION

The rapid market adoption of fast charging and USB-PD standards has significantly amplified the demand for travel adapters with higher power densities. To balance this demand, any reduction in the size of a fully enclosed adapter, achieved through packaging innovation or high-frequency switching, must be coupled with an increase in efficiency to ensure moderate adapter case temperatures. A popular choice in power adapter applications, the single switch quasi-resonant (QR) flyback, exhibits snubber loss, hard switching loss, and excessive EMI, particularly when the switching frequency exceeds 150 kHz [1], [2]. To reduce the volume of passive components, studies have demonstrated the utilization of GaN devices in flyback converters operating at frequencies exceeding 1 MHz [3], [4], [5].

Flyback converters use soft switching methods such as single switch quasi-resonant (QR) flyback, which use

The associate editor coordinating the review of this manuscript and approving it for publication was Jiann-Jong Chen.

resonant circuits that reduce switch loss and increase converter efficiency [6]. Active clamp flyback (ACF) converters feature a clamp circuit that aids in achieving Zero Voltage Switching (ZVS) for the primary power switch, as illustrated in Figure 1. This characteristic makes them particularly suited for high-frequency applications where size reduction and power density increase are desirable, outperforming standard flyback converters [7], [8]. In contrast to conventional flyback converters, the ACF converter integrates a clamp circuit that recycles transformer leakage energy and facilitates ZVS for the primary power switch. This improves the converter's efficiency and makes it more suitable for high-frequency switching operations, thereby increasing power density [9]. A study mentioned in [10] designed a GaN switch based isolated DC-DC converter operating at a 2 MHz frequency for automotive-based low power loads, comparing its pros and cons with a GaN-based ACF converter.

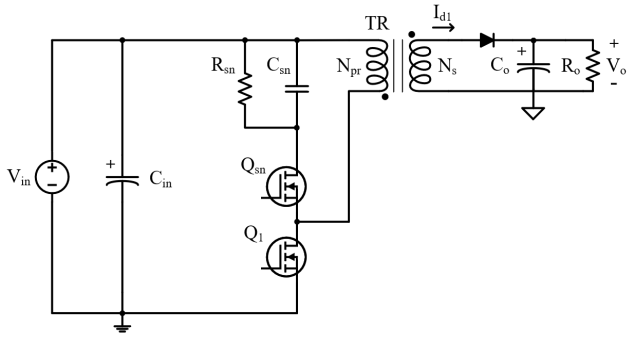

FIGURE 1. Active clamp flyback circuit.

Contemporary trends in power electronics research are not focused on uncovering new topologies, but rather on enhancing existing ones by leveraging the superior capabilities of optimization algorithms to determine the best feasible components. Nature serves as the primary source for population-based meta-heuristic optimization methods such as Genetic Algorithms (GA) and Particle Swarm Optimization (PSO). Owing to their capacity to handle complex problems and exhibit parallelism, these methods have found widespread application in all engineering optimization problems. The population-based meta-heuristic optimization methods demonstrate superior performance in global optimization and are equipped to handle linear or nonlinear, stationary or transient, continuous or discontinuous objective functions [11].

GA and PSO, as the most preferred meta-heuristic optimization methods, have been employed in the design of the CUK converter, thereby enhancing its performance [12]. More reliable and stable Zeta converters have been designed using PSO via optimizing the controller parameters [13]. Reference [14] utilizes an optimization approach grounded in machine learning to select the DC-DC converter's components. Switches and passive components are identified and selected by the optimization algorithm. However, all these studies aim only at finding the optimum design within limited design criteria and objective function.

While existing studies have proposed limited design criteria for power converters, systematic approaches employing multi-objective fitness functions at the system level have begun to emerge, offering a more comprehensive framework. For example, a study detailed in [15] presents a systematic design framework for LLC converters that optimizes resonance frequency and switching frequency limits, ensuring required voltage gains across various quality factors. Similarly, [16] introduces a design tool for gapped core magnetics in LLC converters, selecting the optimal magnetic flux density by minimizing a fitness function that encompasses power loss, cost, and volume, leveraging the Big-Bang Big-Crunch Algorithm.

However, these studies often do not fully address the unique challenges posed by the design of Active Clamp Flyback (ACF) converters, particularly under the rigorous demands of fast charging and USB-PD standards. A multi-objective optimization approach that considers design frequency, power losses, system cost, and volume is crucial for achieving a balanced solution across these parameters, especially given the varied design frequencies required for an ACF converter operating under a wide load range.

In this context, the present paper contributes a novel and comprehensive design and optimization methodology for the selection of power switches, secondary side diodes, and air-gapped magnetics in ACF converters, tailored to a specific database. This method strives to minimize a converter-level fitness function that integrates cost, volume, and losses. Adhering to the proposed methodology, a USB PD converter capable of delivering 5V/9V/15V/20V DC voltages at a maximum power of 65W from a 230 VAC/50 Hz supply has been meticulously designed. The selection of all parameters from a database ensures a rigorous and replicable design process, setting a new benchmark in the field. This paper thus addresses a significant gap in current studies, offering a practical solution to the complex problem of designing efficient, cost-effective, and compact ACF converters suitable for the next generation of fast charging applications.

The paper presents a novel and comprehensive design and optimization methodology for Active Clamp Flyback (ACF) converters, particularly for USB Power Delivery applications. Key contributions include:

1) Development of a multi-objective optimization approach considering design frequency, power losses, system cost, and volume, employing Particle Swarm Optimization.
2) Detailed design process and optimal component selection from a specialized database, ensuring a rigorous and replicable design process.
3) Creation of a converter-level fitness function incorporating cost, volume, and loss considerations.

These points highlight the significant advancements made in ACF converter design, addressing the challenges in fast charging and USB-PD standards.

II. PROPOSED DESIGN AND OPTIMIZATION ALGORITHM

The main objective of an ACF converter design optimization procedure is to ascertain the core size, number of turns, wire size, power devices, and secondary side diodes using both local and global fitness functions that incorporate losses, volume, and cost. Therefore, the design and optimization of an ACF converter can be viewed as a multi-objective optimization problem.

A. PARTICLE SWARM OPTIMIZATION (PSO)

Particle swarm optimization (PSO) is an optimization technique that imitates the hunting behavior of swarms of animals. The number of particles and the maximum number of iterations permitted are decided at the start of the optimization process. The function to be optimized is used to calculate the outcomes of the initial values of particles. The best value in the relevant iteration is referred to as p_{best}, while the best value obtained by optimization is referred to as g_{best}. The p_{best} and g_{best} values are updated following each iteration in order to arrive at the perfect solution. The rate of change of the particles is computed at the end of an iteration, and the new positions of each particle are determined. A new iteration is started with the new positions of the particles. Iteration is continued until the maximum number of iterations is reached. (1)-(3) are PSO equations where i is the number of particles, x is the particle value, v is the rate of change of the particle, c_1 and c_2 are constant values, and $rand_1$ and $rand_2$ are randomly generated values [17].

$$v_{i+1} = v_i + a + b \tag{1}$$

$$a = [c_1 \cdot rand_1 \cdot (p_{best} - x)] \tag{2}$$

$$b = [c_2 \cdot rand_2 \cdot (g_{best} - x)] \tag{3}$$

(1) causes the particle to search for both the local and global best solutions, as well as the best particle solution that is closest to the own best state of particle.

B. MAGNETIC DESIGN

The comprehensive optimization tool uses locally optimized magnetic designs, which compose optimized transformers based on the calculated magnetizing inductance value. The least magnetizing inductance and input-output current values required for the converter to operate continuous conduction mode (CCM) for the ACF converter is given in (4), where D is the duty cycle, f_s is the switching frequency, $v_{in_{max}}$ is the input maximum voltage, P_o is the output power.

$$L_{\min} = \frac{v_{in_{max}}^2 \cdot D^2}{P_o \cdot 2 \cdot f_s} \tag{4}$$

The average value of the primary current ($I_{1_{avg}}$), ripple value of the primary current (ΔI_1), peak value of the primary current ($I_{1_{max}}$), primary current ratio (y_1), ripple factor of the primary current (K_{i_1}) and RMS value of the primary current ($I_{1_{rms}}$) are expressed by (5)-(10) [18].

$$I_{1_{avg}} = \frac{P_o}{D \cdot v_{in_{max}}} \tag{5}$$

$$\Delta I_1 = \frac{v_{in_{max}} \cdot D}{L \cdot f_s} \tag{6}$$

$$I_{1_{max}} = I_{1_{avg}} + \frac{\Delta I_1}{2} \tag{7}$$

$$y_1 = \frac{\Delta I_1}{I_{1_{max}}} \tag{8}$$

$$K_{i_1} = \sqrt{D \cdot \left(1 - y_1 + \left(\frac{y_1^2}{3}\right)\right)} \tag{9}$$

$$I_{1_{rms}} = K_{i_1} \cdot I_{1_{max}} \tag{10}$$

Similarly, the average value of the secondary current ($I_{2_{avg}}$), ripple value of the secondary current (ΔI_2), peak value of the secondary current ($I_{2_{max}}$), secondary current ratio (y_2), ripple factor of the secondary current (K_{i_2}) and RMS value of the secondary current ($I_{2_{rms}}$) are expressed by (11)-(16).

$$I_{2_{avg}} = \frac{P_o}{(1 - D) \cdot v_o} \tag{11}$$

$$\Delta I_2 = a \cdot \Delta I_1 \tag{12}$$

$$I_{2_{max}} = I_{2_{avg}} + \frac{\Delta I_2}{2} \tag{13}$$

$$y_2 = \frac{\Delta I_2}{I_{2_{max}}} \tag{14}$$

$$K_{i_2} = \sqrt{(1 - D) \cdot \left(1 - y_2 + \left(\frac{y_2^2}{3}\right)\right)} \tag{15}$$

$$I_{2_{rms}} = K_{i_2} \cdot I_{2_{max}} \tag{16}$$

The formulas for calculating copper (P_{Cu}) and core losses (P_{Fe}) are (17)-(20), where a is the resistance term for copper loss (Ω), b is the temperature term for copper loss, MLT is the average turn length of transformer (m), N is the number of turn, ρ is the resistivity value (Ω/m), α_{20} is the heat coefficient at 20°C (1/°C), T_{max} is the maximum temperature (°C), f is the switching frequency (Hz) and ΔB is the flux density ripple from peak to peak (T). The K_c, α and β coefficients are produced using the P (W/mm^3) - B (mT) graphs for various frequency values provided by the manufacturer data, and the core loss is calculated using the Steinmetz equation.

$$P_{Cu} = a \cdot b \cdot I^2 \tag{17}$$

$$a = MLT \cdot N \cdot \rho_{20} \tag{18}$$

$$b = \left[1 + \alpha_{20} \cdot (T_{max} - 20°\mathrm{C})\right] \tag{19}$$

$$P_{Fe} = K_c \cdot f^{\alpha} \cdot \left(\frac{\Delta B}{2}\right)^{\beta} \tag{20}$$

The thermal resistances (R_Θ) of the cores are calculated using the empirical method provided in (21), where V_c is the core volume (m^3), for natural convection cooling in order to estimate the temperature rise of the magnetic components, and temperature rise is checked by utilizing (22). As a design restriction, the maximum temperature rise (ΔT) is limited to 80°C. P_D is the maximum power for transformer at 80°C

temperature limit.

$$R_{\Theta} = \frac{0.06}{\sqrt{V_c}} \tag{21}$$

$$P_D = \frac{\Delta T}{R_{\theta}} \tag{22}$$

The optimization algorithm sweeps the switching frequency to find the optimal design by minimizing a local fitness function, which includes loss, cost and volume of the transformer. The local fitness function is given with (23), where V_{trf}, C_{trf}, and P_{trf} are the volume, cost and power loss of the selected transformer for the relevant frequency, respectively. $V_{trf_{best}}$, $C_{trf_{best}}$, and $P_{trf_{best}}$ are highest volume, cost and power loss of the selected transformer for the relevant frequency, respectively. α_1, α_2 and α_3 are the optimization coefficient for volume, cost and power loss of the transformer, respectively. The design obtained for the minimum value of the local fitness function is accepted as the optimum design.

$$f_{opt_{trf}} = \left(\alpha_1 \cdot \frac{V_{trf}}{V_{trf_{best}}}\right) + \left(\alpha_2 \cdot \frac{C_{trf}}{C_{trf_{best}}}\right) + \left(\alpha_3 \cdot \frac{P_{trf}}{P_{trf_{best}}}\right) \tag{23}$$

In order to include the cost in the local fitness function, the winding copper cost, material cost based on volume, and labor costs are extracted from different suppliers. Total core, winding and labor costs can be calculated as in (24)-(26), where $\sigma_{core,x}$, $\sigma_{wdg,x}$ and $\sigma_{lab,x}$ are the specific costs per weight considering different magnetic core and the winding types. $\sum^{fc}_{core,x}$, $\sum^{fc}_{wdg,x}$ and $\sum^{fc}_{lab}$ indicate the fixed costs for the magnetic cores including the coil formers, connectors, and labor, where N_{stack} represents the stacking factor. The winding Cu cost, material cost dependent on volume, and labor prices are extracted from several vendors in order to integrate the cost in the optimization function. The calculation of transformer costs is given as in (27). At (27), the fixed cost due to the stacking of the core (C_{core}), the windings cost ($C_{winding}$), and labor cost (C_{labor}) are used for providing the local fitness function of the transformer. All numerical data retrieved from manufacturer is given in Table 1 [19].

$$C_{core} = N_{stack} \cdot \sum_{core,x}^{fc} + \sigma_{core,x} \cdot W_{core} \tag{24}$$

$$C_{wdg} = \sum_{wdg,x}^{fc} + \sigma_{wdg,x} \cdot W_{wdg} \tag{25}$$

$$C_{wdg} = \sum_{lab}^{fc} + \sigma_{lab,x} \cdot W_{wdg} \tag{26}$$

$$C_{trf} = C_{core} + C_{wdg} + C_{lab} \tag{27}$$

C. POWER SWITCHES AND DIODE SELECTION

In this study, GaN devices were chosen for main and clamp switches because they operate with minimal loss at high frequency. The total power losses and cost values are used in the local optimization algorithm to determine the appropriate switches for the ACF converter. Switch power losses can be expressed as the sum of conduction loss, switching loss, gate loss, and reverse recovery loss [15].

TABLE 1. Retrieved numerical cost model data from several winding, core and inductor manufacturers.

Specific Cost	Values
$\sum^{fc}_{core,x}$ (€/unit)	0.08
$\sigma_{core,x}$ (€/kg)	7.5
$\sum^{fc}_{wdg,x}$ (€/unit)	0.25
$\sigma_{wdg,x}$ (€/kg)	16.5
$\sum^{fc}_{lab}$ (€/unit)	0.75
$\sigma_{lab,x}$ (€/kg)	7

While calculating the conduction loss, the resistance value of the switch at the on position R_{dson} and the RMS value of the current passing through the switch $I_{ds_{rms}}$ are used. The equation for the conduction loss is given as in (28).

$$P_{con} = R_{dson} \cdot I^2_{ds_{rms}} \tag{28}$$

The switching loss can be calculated using (29) where; V_{ds} is the voltage for the switch-off position (V), I_{ds} is the average value of the current passing through the switch (A), t_r is the rise time of the current passing through the switch when turning on in seconds, t_f is the falling time of the current passing through the switch when turning off in seconds.

$$P_{sw} = \left(\frac{1}{2}\right) \cdot V_{ds} \cdot I_{ds} \cdot (t_r + t_f) \cdot f_s \tag{29}$$

The power loss due to the parasitic capacitances in the gate can be calculated as in (30) where; Q_g is the charge for the gate of the switch in Coulombs, and $V_{gs_{max}}$ is the max. gate-source voltage in Volts.

$$P_g = Q_g \cdot V_{gs_{max}} \cdot f_s = C_g \cdot V^2_{gs} \cdot f_s \tag{30}$$

The power loss for anti-parallel body diode is known as the reverse recovery loss and is calculated as in (31) where; Q_{rr} is the reverse recovery charge value of the switch in Coulombs, and V_{sd} is the voltage drop on the diode in Volts. The total power loss on switch is given as in (32).

$$P_{rr} = \left(\frac{1}{2}\right) \cdot Q_{rr} \cdot V_{sd} \cdot f_s \tag{31}$$

$$P_{tot_{switch}} = P_{con} + P_{sw} + P_g + P_{rr} \tag{32}$$

Volume and power density factors play a significant role in USB PD converter applications. Numerous approaches are used for this kind of consumer product design to maintain the temperature rise in the switches at specific levels in order to reduce expenses and improve volume and power density values. They include choosing the right amount of the surface space required to dissipate the heat in the switch selection, designing the PCB by taking thermal resistances into consideration, and reducing the losses of the main

switch by utilizing auxiliary switches. Due to the volume constraints in this study, the PCB layout was developed to dissipate the heat generated on the switches instead of using a heatsink.

After the switch selection for whole frequency range, the most optimum design is obtained by using the local switch fitness function including the cost and power loss values. The local fitness function used for optimization is given as in (33) where C_{switch} and P_{switch} are the total cost and power losses of the selected switch for the relevant frequency, $C_{switch_{best}}$ and $P_{switch_{best}}$ are the highest total cost and power loss of the selected switch for the relevant frequency, respectively. β_1 and β_2 are the optimization coefficient for cost and power loss of the switch, respectively.

$$f_{opt_{switch}} = \left(\beta_1 \cdot \frac{C_{switch}}{C_{switch_{best}}}\right) + \left(\beta_2 \cdot \frac{P_{switch}}{P_{switch_{best}}}\right) \tag{33}$$

The total power loss and cost values in the database of diodes are used to choose the best diode. Conduction loss, switching loss, and reverse recovery loss are the three types of power losses generated by diodes. The cost value is obtained from the suppliers. While calculating the conduction loss of a diode as in (34), the resistance value of the diode (R_d), the voltage drops of the diode (V_f), the RMS value of the current passing through the diode ($I_{d_{rms}}$) and its average value ($I_{d_{avg}}$) are used.

$$P_{con_d} = (R_d \cdot I_{d_{rms}}^2) + (V_f \cdot I_{d_{avg}}) \tag{34}$$

The switching loss of a diode can be calculated as in (35) where f_s is the switching frequency, Q_c is the junction charge value of the diode, and V_d is the diode voltage.

$$P_{sw_d} = Q_c \cdot V_d \cdot f_s \tag{35}$$

When changing state from the conduction state to the cut-off state due to the p-n-junction structure of the diode, a reverse current is passed through it. The power loss caused by this current can be calculated as in (36) where Q_{rr} is the reverse recovery charge value of the diode.

$$P_{rr_d} = \left(\frac{1}{2}\right) \cdot Q_{rr} \cdot V_d \cdot f_s \tag{36}$$

The total power loss dissipating the diode is given by the sum of the power losses as in (37).

$$P_{tot_{diode}} = P_{con_d} + P_{sw_d} + P_{rr_d} \tag{37}$$

After the diode selection for whole frequency range, the most optimum design is obtained by using the local fitness function including the cost and power loss values of the diode. The function used for optimization is given as in (38) where C_{diode} and P_{diode} are the total cost and power losses of the selected diode for the relevant frequency, $C_{diode_{best}}$ and $P_{diode_{best}}$ are the highest total cost and power losses of the selected diode for the relevant frequency, respectively. γ_1 and γ_2 are the optimization coefficient for cost and power loss of the diode, respectively.

$$f_{opt_{diode}} = \left(\gamma_1 \cdot \frac{C_{diode}}{C_{diode_{best}}}\right) + \left(\gamma_2 \cdot \frac{P_{diode}}{P_{diode_{best}}}\right) \tag{38}$$

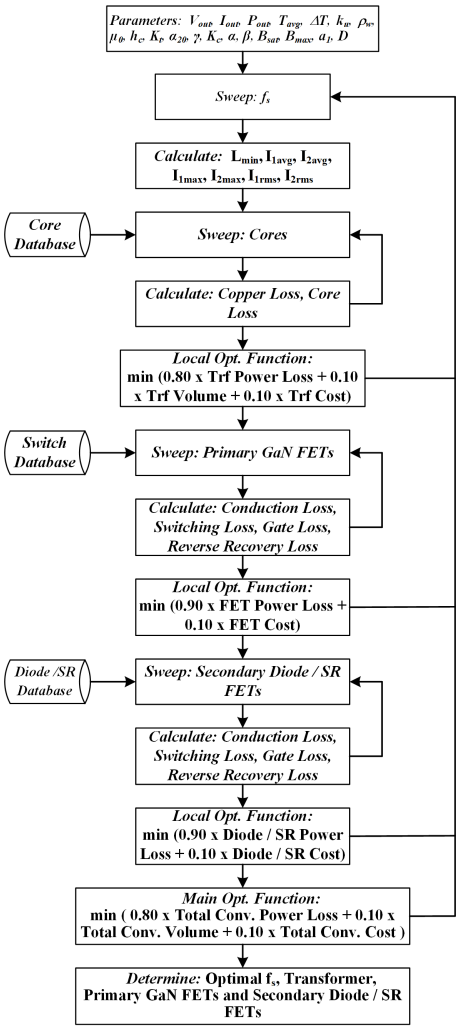

FIGURE 2. Proposed algorithm flow chart.

In this study, a design and optimization algorithm for USB PD devices is proposed under the constraints of loss, cost, and volume associated with the ACF converter. The total fitness function of the converter is obtained by summing the local fitness functions in each component of the converter. These local fitness functions include:

1) Transformer volume, core, transformer copper losses, and the transformer cost.
2) Conduction, switching, reverse recovery, and gate losses of the switch and the switch's cost.
3) Conduction, switching, and reverse recovery losses of the diode and the diode's cost.

After obtaining the volume, cost, and losses of the locally optimized power devices and the transformer, the converter level global fitness function is calculated. This creates a design space populated with locally optimized designs. The converter level global fitness function, given in equation (39), is applied to all magnetic cores, switches, and diodes in the database. The designs that yield the smallest fitness function can be chosen as the best.

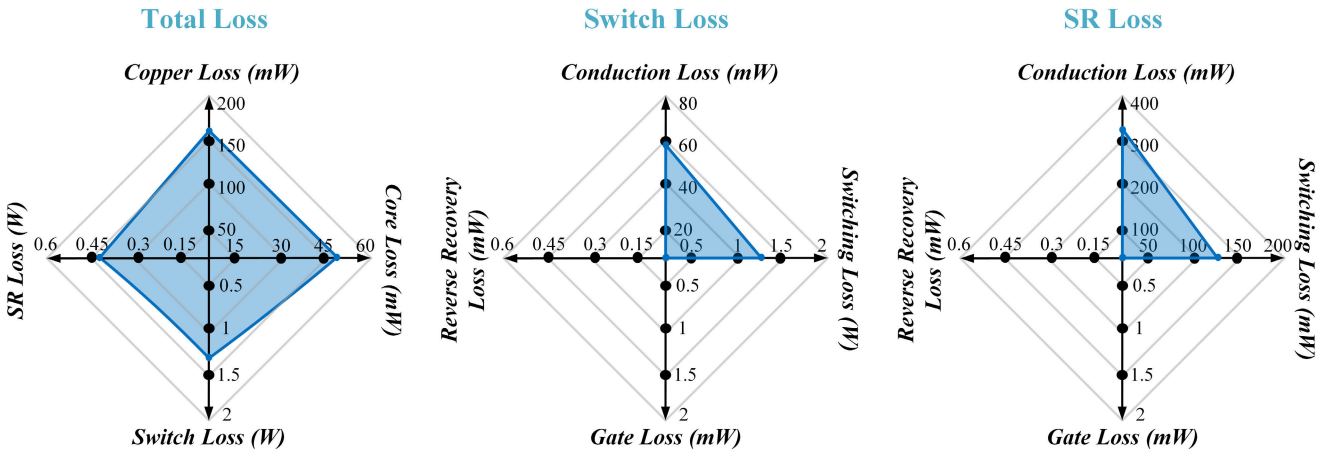

FIGURE 3. Losses of flyback converter obtained after optimization under volume constraint.

Each value calculated in the function is normalized, providing the minimum volume, power loss, and cost for the selection of the magnetic core, switch, and diode. The flowchart of the proposed design and optimization algorithm is illustrated in Figure 2.

$$f_{opt_{flyback}} = f_{opt_{trf}} + f_{opt_{switch}} + f_{opt_{diode}} \tag{39}$$

Given that the suggested converter design and optimization is intended for small-scale, compact, and cost-effective USB-PD applications, it is proposed that no heatsink is necessary for the power devices within the converter. Additionally, the power switches should possess inherent cooling capabilities. As the converter lacks a heatsink structure, the transformer emerges as the largest component in terms of volume. Consequently, in (39), solely the volume of the transformer is considered for optimization, as there exists no other component aside from the transformer wherein volume reduction is feasible.

III. RESULTS AND DISCUSSION

This study aims to optimize the transformer, switch, and synchronous rectifier/diode elements of the ACF converter concerning volume, efficiency, and cost for a given database from different manufacturer. The database contains 29 different switches for the main and active clamp switch on the primary side and 80 different switches/diodes for the synchronous rectifier/diode on the secondary side. The power losses of the output diode can be reduced by using a synchronous rectifier (SR) for flyback converters, so the proposed algorithm can select the synchronous rectifier or diode for secondary side rectifier according to the design criteria. Besides, the EE type cores in this database are linked to the four different materials N87, 3C90, 3C92, 3C94, 3C95, and 3F36. These cores are available in a range of 21 different volume sizes, ranging from 559 mm^3 (13/06/06) to 52000 mm^3 (55/28/25), for a total of 64 separate core configurations. The algorithm sweeps the frequency between 50-800 kHz in the outer loop. The optimization algorithm's fitness function incorporates weights attributed to power loss-volume-cost. These weights were assigned as 10%-80%-10% under limitations related to volume, 10%-10%-80% under constraints concerning cost, and 80%-10%-10% under restrictions linked to yield. These allocations of weights may be subject to modification based on user-specified demands. The ACF converter is designed using the particle swarm optimization method, with the pre-optimization design parameters provided in Table 2.

TABLE 2. Pre-design optimization parameters.

Symbol	Quantity	Value
$V_{in_{rms}}$	AC Input RMS Voltage	230 V_{AC}
$I_{in_{rms}}$	AC Input RMS Current	0.3731 A
V_{out}	DC Output Voltage	9/12/15/20 V_{DC}
I_{out}	Max. DC Output Current	3.25 A
P_{out}	Max Output Power	65 W
T_{amb}	Ambient Temperature	20°C
ΔT	Temperature Rise	60°C
f_s	Switching Frequency Range	50-800 kHz
D_{min}	Minimum Duty Cycle	33.96%
L_{mag}	Magnetization Inductance	0.7551 mH
a_1	Transformation Ratio for Output	8
a_{aux_1}	Transformation Ratio for Aux. 1	4
a_{aux_2}	Transformation Ratio for Aux. 2	2

The transformer parameters resulting from the optimization under volume, cost, and efficiency constraints are presented in Table 3 respectively. The optimal parameters for the main switch, active clamp switch, and SR or diode are provided in Table 4 respectively for volume, cost, and efficiency constraints.

For volume constraint, the algorithm suggests using a 3C94, E-25/13/7 core, NV6117, NV6115, and BSC093N 15NS5 MOSFETs on the main switch, active clamp switch, and SR respectively. Under cost constraint, the algorithm recommends a 3F36, E-35/18/10 core, GS-065-004-1-L on

TABLE 3. Optimum transformer parameters under different constraints.

Constraint	Transformer Core	Primary Winding Number	Secondary Winding Number	Auxiliary 1 Winding Number	Auxiliary 2 Winding Number	Copper Loss (mW)	Core Loss (mW)	Total Loss (mW)	Maximum Allow-able Loss (mW)
Volume	3C94, E-25/13/7	67	9	36	18	160.465	50.267	210.732	864.6
Cost	3F36, E-35/18/10	106	14	56	28	344.663	25.790	370.453	1.420
Efficiency	3F36, E-42/21/10	106	14	56	28	100.663	30.898	131.561	1.420

TABLE 4. Optimum parameters for different types of switches under various constraints.

Constraint	Switch Type	Component	Conduction Loss (mW)	Switching Loss (mW)	Gate Loss (mW)	Reverse Recovery Loss (mW)	Total Loss (W)
Volume	Main Switch	NV6117	59.871	1240	0	0	1.299
	Active Clamp Switch	NV6115	0.306	1240	0	0	1.240
	SR Switch	BSC093N15NS5	310.015	128.593	0	0	0.438
Cost	Main Switch	GS-065-004-1-L	89.450	1132	0	0	1.221
	Active Clamp Switch	GS-065-004-1-L	0.316	1132	0	0	1.132
	Diode	IDH06G65C6	0.664	128.593	-	0	0.793
Efficiency	Main Switch	NV6123	79.363	1034	0	0	1.113
	Active Clamp Switch	NV6115	0.133	1034	0	0	1.034
	Diode	GE06MPS06E	0.537	42.329	-	0	0.579

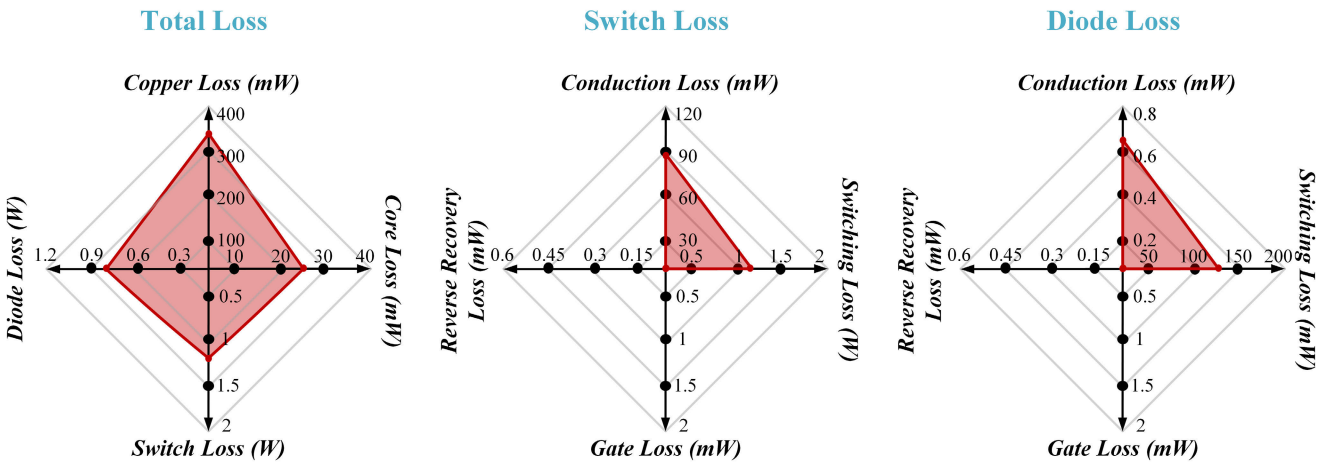

FIGURE 4. Losses of flyback converter obtained after optimization under cost constraint.

the main switch and active clamp switch, and IDH06G65C6 for the diode. Finally, for efficiency constraint, the algorithm advises using a 3F36, E-42/21/20 core and NV6123, NV6115, and GE06MPS06E on the main switch, active clamp switch, and diode respectively.

Comprehensive assessment of power dissipation within the transformer, switches, and SR/diode is presented through radar charts, featured in Figures 3, 4, and 5, corresponding to the constraints of volume, cost, and efficiency. To enhance the scrutiny of power loss distribution specifically pertaining to switches and SR, both conduction and switching losses are graphically represented within Figure 3, 4, and 5, aligning with the constraints of volume, cost, and efficiency, respectively.

Subject to a volume constraint, the optimal values for design parameters emerge as 227.46 kHz, \$16.13, and

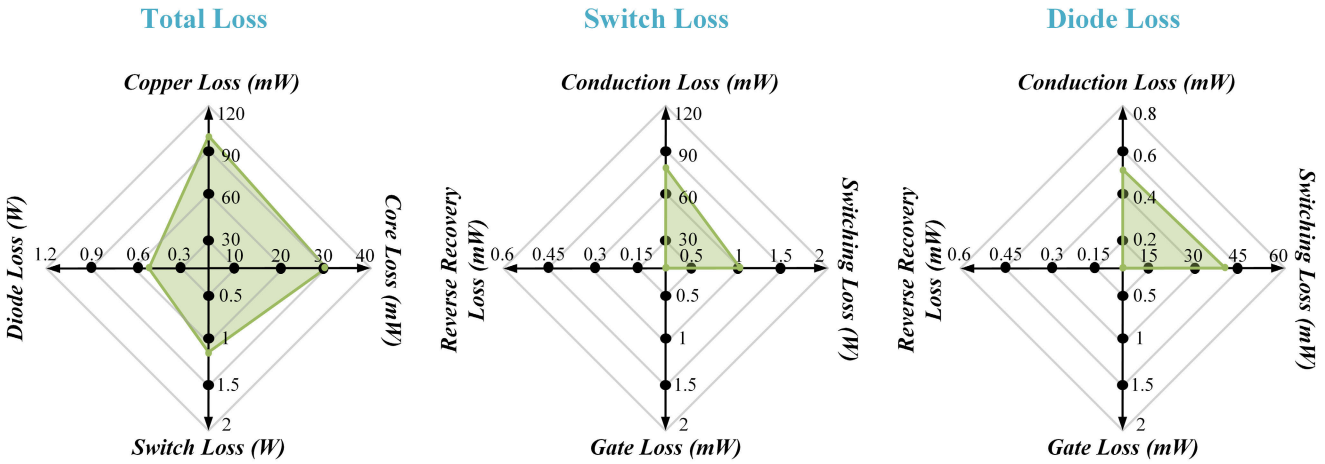

FIGURE 5. Losses of flyback converter obtained after optimization under efficiency constraint.

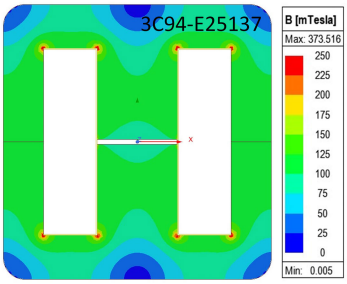

FIGURE 6. Magnetic flux density for selected transformer.

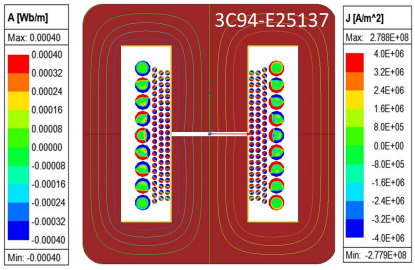

FIGURE 7. Magnetic flux distribution and current density for selected transformer.

93.83% in relation to frequency, cost, and efficiency respectively. In the scenario of a cost constraint, the optimal design parameters manifest as 174.87 kHz, \$14.92, and 94.86% for frequency, cost, and efficiency, in that order. Similarly, when prioritizing efficiency constraints, the optimum design parameters materialize as 152.34 kHz, \$16.75, and 95.61% for frequency, cost, and efficiency, respectively.

A transformer model was designed and validated using Ansys Electronics Desktop and Simplorer environment. The aim of the study was to optimize the performance of transformers by carefully considering various parameters such as size, shape, and material selection.

The designed transformers were characterized by their parameters, which are listed in Table 3. To verify the model used in the optimization framework, co-simulations were conducted using Ansys Electronics Desktop and Simplorer environment. Specifically, the 3C94-E25137 transformer was selected for finite element analysis (FEA) and Simplorer co-simulations.

For FEA, a two-dimensional (2D) transient magnetic model was employed to compare outcomes and operational quantities, such as magnetic flux density, current density, and losses. The magnetic flux distributions, which shows that the flux is denser towards the winding window area

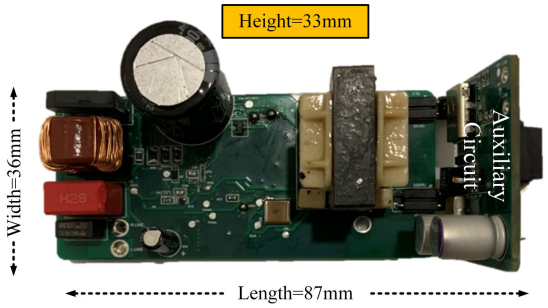

FIGURE 8. Prototype of the designed active clamp flyback converter.

of the core where the flux path length is minimal, and crowded on the inner edge of the core are displayed in Figure 6.

The magnetic flux lines and current density distributions, which are shown in Figure 7, were examined. The analysis revealed that the current becomes crowded on the conductors near the air gap and on the surfaces where the primary and secondary windings face each other. Valuable insights into the performance of designed transformers and the accuracy of the model used in the optimization framework were provided. The magnetic flux density, current density,

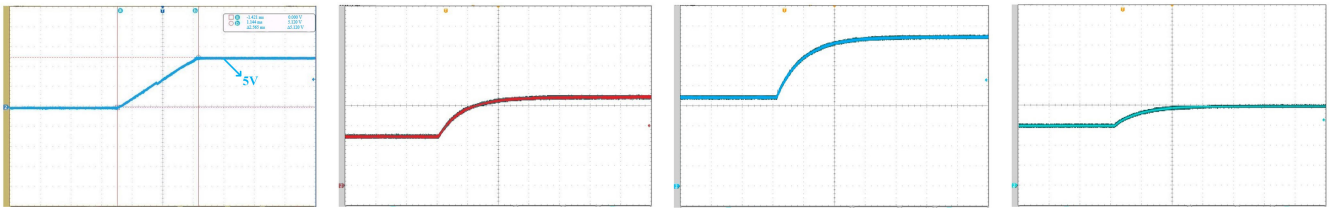

FIGURE 9. Experimental waveforms output voltage transitions for; (a) start-up at no load, (b) 5 V to 9 V transition at no load, (c) 9 V to 15 V transition at no load, (d) 15 V to 20 V transition at no load.

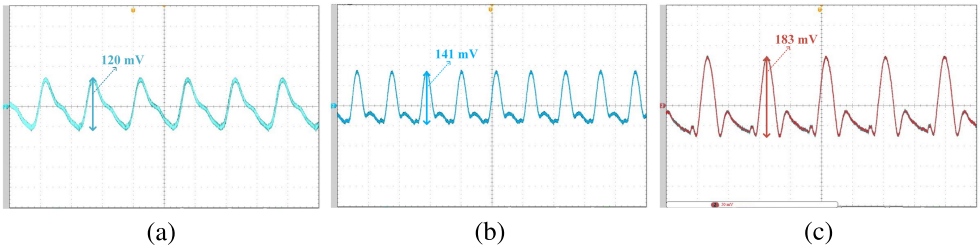

FIGURE 10. Experimental waveforms output voltage ripple for; (a) 5 V - 3 A, (b) 9 V - 3 A, (c) 20 V - 3 A.

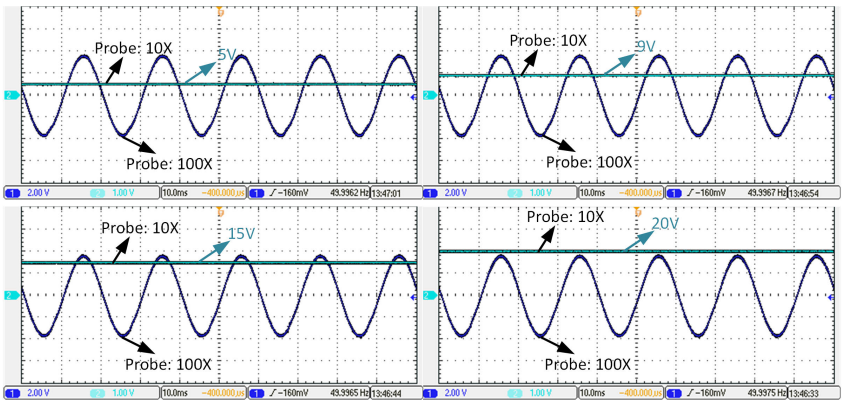

FIGURE 11. AC-DC conversion waveforms under different output voltage.

and losses are crucial factors that affect the efficiency and reliability of transformers. Therefore, the findings of this study can be used to optimize the design of transformers and improve their performance in power systems.

IV. EXPERIMENTAL RESULTS

In this study, the design optimization of an active clamp flyback converter for USB loads was accomplished using the particle swarm optimization method, a meta-heuristic method. Optimal design of the converter with regards to efficiency, cost, and volume constraints was obtained through design optimization, and the resulting design parameters are presented in the previous section.

A converter circuit was constructed by choosing one of the optimized designs. The converter was planned and manufactured as two sub circuits. Images of the circuits are illustrated in Figure 8.

Figure 9 showcases the experimental waveforms depicting the output voltage transitions of the optimized Active Clamp Flyback (ACF) converter under various no-load conditions. Figure 9(a) illustrates the converter's startup behavior, achieving a stable 5V output with minimal overshoot, indicative of the robustness of the design during initial power-up. Figure 9(b) reveals the transition from 5V to 9V, demonstrating the converter's quick response to step changes in voltage demands while maintaining a flat output, which is critical for the stability of USB PD devices. In Figure 9(c), the transition from 9V to 15V is similarly swift and stable, further confirming the converter's versatility across different voltage levels. Lastly, Figure 9(d) exhibits the transition from 15V to 20V, underscoring the converter's capability to scale to higher voltages without load, which is essential for fast-charging applications that require variable output voltages.

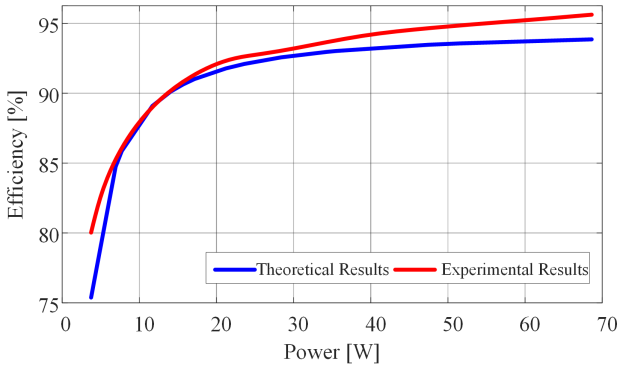

FIGURE 12. Comparison of theoretical and experimental results.

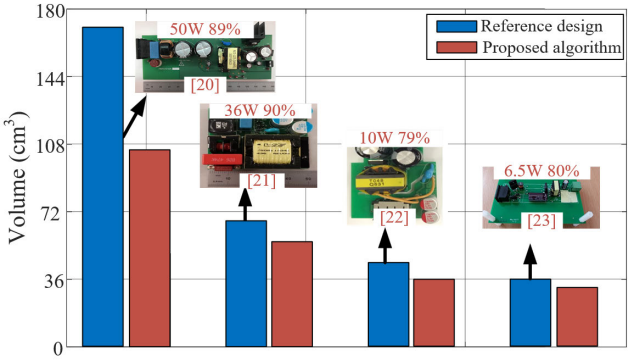

FIGURE 14. Comparison of flyback prototypes in literature [20], [21], [22], [23].

Figure 10 presents the experimental output voltage ripple waveforms for the ACF converter at different load conditions. In Figure 10(a), the converter exhibits a ripple of 120 mV at a 5V - 3A load, illustrating good performance in minimizing fluctuations within the standard operating range. Figure 10(b) shows a slightly higher ripple of 141 mV at a 9V - 3A load, still within acceptable limits for USB PD applications and indicative of the converter's reliable output under mid-range voltages. Finally, Figure 10(c) depicts the ripple at the highest tested voltage of 20V - 3A load, with a ripple of 183 mV. While this represents an increase, it remains within a reasonable range, considering the higher output voltage. These ripples are critical indicators of the stability and efficiency of the power converter, and the results demonstrate the converter's capacity to maintain a stable output across a variety of loads, a paramount feature for versatile fast-charging solutions. In addition, AC-DC conversion of designed ACF converter waveforms under different output voltage are given in Figure 11.

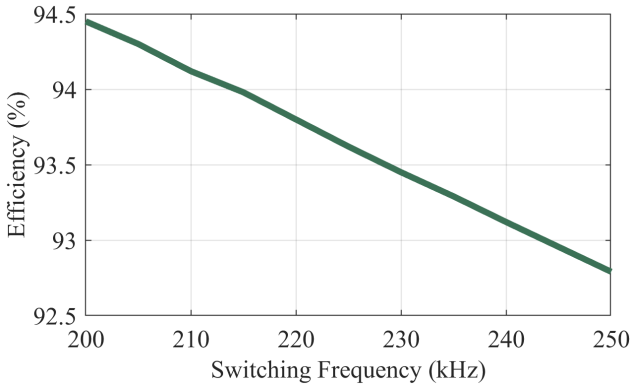

FIGURE 13. Frequency vs. efficiency graph for optimized design under volume constraint.

Efficiency values were computed as a result of the flyback converter design and optimization, and these values, acquired from experimental results, are exhibited in Figure 12. As seen, the two curves in the figure have analogous waveforms and the efficiency augments with the load until it hits its nominal value. Both curves decline with similar waveforms when the rated load is surpassed. The experimental results exhibit higher values than the theoretical ones, thus verifying the accuracy and reliability of the design optimization algorithm.

Converters may not operate with precision to two decimal point at the correct fixed frequency. Figure 13 illustrates how the efficiency will change under a variation of ±10% in the switching frequency. As depicted in Figure 13, a 10% alteration in the switching frequency corresponds to a maximum 1% change in the efficiency value.

To demonstrate the benefits of the suggested method, the recommended optimization technique has been implemented using volume-weighted design parameters for four benchmark designs presented in [20-23] with 50, 36, 10, 6.5 W output power and an output voltage range of 24-12-5-15 V. Efficiency and boxed volume are compared for each design, and the results are displayed in Figure 14 as stacked bar charts. The proposed algorithm has provided a volumetric advantage of 37.33% in the 50W design, 16.66% in the 36W design, 21.98% in the 10W design, and 13.33% in the 6.5W design.

V. CONCLUSION

In this study, an optimized Active Clamp Flyback (ACF) converter for USB Power Delivery applications has been developed. Utilizing Particle Swarm Optimization (PSO) has led to a highly efficient, compact and cost-efficient design that is capable of delivering multiple DC outputs at a maximum power of 65W, with a peak efficiency of 95.61%. Implementing the gallium nitride (GaN) technology was fundamental in lowering the cost to $14.92 and attaining an operational frequency of 227.46 kHz.

Considering that fast charging operation is a challenging application, the achievements made in this study are significant. The converter's performance, characterized by its cost-efficiency and compact design, showcases the potential to influence a broad spectrum of USB-PD systems.

The methodologies and findings of this paper not only enhance the current state of ACF converter designs but also provide a scalable model that can adapt to evolving technologies and market needs. Looking ahead, the framework established here is expected to inspire further research, particularly in the optimization of power electronics to meet emerging global standards for efficiency and sustainability. The ACF converter design showcased here demonstrates the importance of thorough optimization for practical, efficient, and cost-effective power conversion systems.

REFERENCES

[1] J. Yao, Y. Li, S. Wang, X. Huang, and X. Lyu, "Modeling and reduction of radiated EMI in a GaN IC-based active clamp flyback adapter," *IEEE Trans. Power Electron.*, vol. 36, no. 5, pp. 5440–5449, May 2021, doi: 10.1109/tpel.2020.3032644.

[2] Z. Ma, S. Wang, H. Sheng, and S. Lakshmikanthan, "Modeling, analysis and mitigation of radiated EMI due to PCB ground impedance in a 65W high-density active-clamp flyback converter," *IEEE Trans. Ind. Electron.*, vol. 70, no. 12, pp. 12267–12277, Dec. 2023, doi: 10.1109/TIE.2023.3239904.

[3] S. Gao, H. Song, Y. Wang, R. Xu, and D. Xu, "A secondary-resonance MHz active-clamp flyback converter with partial power processing," *IEEE Trans. Ind. Appl.*, vol. 58, no. 6, pp. 7988–7997, Nov. 2022, doi: 10.1109/TIA.2022.3194868.

[4] Y.-C. Liu, B.-S. Huang, C.-H. Lin, K. A. Kim, and H.-J. Chiu, "Design and implementation of a high power density active-clamped flyback converter," in *Proc. Int. Power Electron. Conf. (IPEC-Niigata -ECCE Asia)*, Niigata, Japan, May 2018, pp. 2092–2096, doi: 10.23919/IPEC.2018.8507824.

[5] M. Li, Z. Ouyang, and M. A. E. Andersen, "Analysis and optimal design of high-frequency and high-efficiency asymmetrical half-bridge flyback converters," *IEEE Trans. Ind. Electron.*, vol. 67, no. 10, pp. 8312–8321, Oct. 2020, doi: 10.1109/TIE.2019.2950845.

[6] C. Wang, S. Xu, W. Shen, S. Lu, and W. Sun, "A single-switched high-switching-frequency quasi-resonant flyback converter," *IEEE Trans. Power Electron.*, vol. 34, no. 9, pp. 8775–8786, Sep. 2019, doi: 10.1109/TPEL.2018.2884937.

[7] L. Huber, M. M. Jovanovic, H. Song, D. Xu, A. Zhang, and C.-C. Chang, "Flyback converter with hybrid clamp," in *Proc. IEEE Appl. Power Electron. Conf. Exposit. (APEC)*, San Antonio, TX, USA, Mar. 2018, pp. 2098–2103, doi: 10.1109/APEC.2018.8341306.

[8] M. Ursino, S. Saggini, R. Specogna, A. Bianco, F. Ciappa, and G. Scappatura, "A novel mixed planar litz transformer for high frequency active clamp flyback converters," in *Proc. IEEE Appl. Power Electron. Conf. Exposit. (APEC)*, New Orleans, LA, USA, Mar. 2020, pp. 1327–1332, doi: 10.1109/APEC39645.2020.9124197.

[9] S. Xu, Q. Qian, R. Shi, S. S. Shah, Q. Liu, S. Lu, and W. Sun, "Sampled-data modeling for PCM and ZVS controlled critical conduction mode (CrCM) active clamp flyback (ACF) converter at variable switching frequency," *IEEE Trans. Circuits Syst. I, Reg. Papers*, vol. 67, no. 10, pp. 3588–3600, Oct. 2020, doi: 10.1109/TCSI.2020.2993256.

[10] S. Cabizza, G. Spiazzi, and L. Corradini, "GaN-based isolated resonant converter as a backup power supply in automotive subnets," *IEEE Trans. Power Electron.*, vol. 38, no. 6, pp. 7362–7373, Jun. 2023, doi: 10.1109/TPEL.2023.3245561.

[11] S. E. De León-Aldaco, H. Calleja, and J. Aguayo Alquicira, "Metaheuristic optimization methods applied to power converters: A review," *IEEE Trans. Power Electron.*, vol. 30, no. 12, pp. 6791–6803, Dec. 2015, doi: 10.1109/TPEL.2015.2397311.

[12] M. R. Yousefi, S. A. Emami, S. Eshtehardiha, and M. B. Poudeh, "Particle swarm optimization and genetic algorithm to optimizing the pole placement controller on cuk converter," in *Proc. IEEE 2nd Int. Power Energy Conf.*, Johor Bahru, Malaysia, Dec. 2008, pp. 1461–1465, doi: 10.1109/PECON.2008.4762707.

[13] M. M. Nishat, M. R. K. Shagor, H. Akter, S. A. Mim, and F. Faisal, "An optimal design of PID controller for DC–DC zeta converter using particle swarm optimization," in *Proc. 23rd Int. Conf. Comput. Inf. Technol. (ICCIT)*, DHAKA, Bangladesh, Dec. 2020, pp. 1–6, doi: 10.1109/ICCIT51783.2020.9392676.

[14] S. Reese, T. Byrd, J. Haddon, and D. Maksimovic, "Machine learning-based component figures of merit and models for DC–DC converter design," in *Proc. IEEE Design Methodologies Conf. (DMC)*, Bath, United Kingdom, Sep. 2022, pp. 1–6, doi: 10.1109/DMC55175.2022.9906474.

[15] A. Lordoglu, M. O. Gulbahce, D. A. Kocabas, and S. Dusmez, "A holistic design optimization method for LLC converters in light electric vehicle chargers," *IEEE Trans. Transport. Electrific.*, early access, Jul. 24, 2024, doi: 10.1109/TTE.2023.3298170.

[16] A. Lordoglu, M. O. Gulbahce, D. A. Kocabas, and S. Dusmez, "A new optimization method for gapped and distributed core magnetics in LLC converter," *IEEE Access*, vol. 11, pp. 14061–14072, 2023, doi: 10.1109/ACCESS.2023.3242869.

[17] Y. Shi and R. Eberhart, "A modified particle swarm optimizer," in *Proc. IEEE Int. Conf. Evol. Comput. Proceedings. IEEE World Congr. Comput. Intell.*, Anchorage, AK, USA, 1998, pp. 69–73, doi: 10.1109/ICEC.1998.699146.

[18] W. G. Hurley and W. H. Wölfle, *Transformers and Inductors for Power Electronics: Theory, Design and Applications*. Hoboken, NJ, USA: Wiley, 2013.

[19] R. M. Burkart, "Advanced modeling and multi-objective optimization of power electronic converter systems," Doctoral dissertation, Dept. Inf. Technol. Elect. Eng., ETH Zurich, Zürich, Switzerland, 2016.

[20] Texas Instruments. *PMP21516*. Accessed: Jan. 20, 2024. [Online]. Available: https://www.ti.com/tool/PMP21516

[21] Texas Instruments. *PMP9730*. Accessed: Jan. 20, 2024. [Online]. Available: https://www.ti.com/tool/PMP9730

[22] Texas Instruments. *PMP11612*. Accessed: Jan. 20, 2024. [Online]. Available: https://www.ti.com/tool/PMP11612

[23] Texas Instruments. *TIDA-00628*. Accessed: Jan. 20, 2024. [Online]. Available: https://www.ti.com/tool/TIDA-00628

OMER SAID AYDIN received the B.Sc. degree in electrical engineering from Yildiz Technical University (YTU), İstanbul, Turkey, in 2017. He is currently pursuing the M.Sc. degree in electrical engineering with Istanbul Technical University (ITU), İstanbul. Since 2017, he has been an Electronic Hardware Engineer with Baykar Defense, İstanbul. His research interests include design and optimization of DC/DC converters, high efficiency solutions for DC/DC converters, and power electronic converters.

ABDULSAMED LORDOGLU (Member, IEEE) received the B.S. degree in electrical engineering from Yildiz Technical University (YTU), İstanbul, Turkey, in 2016, and the M.Sc. degree from the Electrical Engineering Program, Institute of Science and Technology, Istanbul Technical University (ITU), in 2019. He is currently pursuing the Ph.D. degree with the Electrical Engineering Program. He was a Research Assistant with the Department of Electrical Engineering, Electrical and Electronic Faculty, YTU, between 2017 and 2021. He is currently a Lecturer with the Energy Institute, ITU. His main research interests include high power density solutions for DC/DC resonant converters and the design and optimization of resonant converters for electric vehicles, electrical machines and power converters, harmonics, and acoustic noise in electrical machines.

MELTEM LORDOGLU received the B.S. degree in bioengineering and electrical engineering from Yildiz Technical University (YTU), İstanbul, Turkey, in 2017 and 2018, respectively, and the M.Sc. degree from the Electrical Engineering Program, Institute of Science and Technology, Istanbul Technical University (ITU), in 2022, where she is currently pursuing the Ph.D. degree. She is currently a Research Assistant with the Department of Electrical Engineering, Electrical and Electronic Faculty, ITU. Her main research interests include design and optimization of magnetics of biomedical or electromagnetic systems, such as assistive hearing loops, power converters, and electrical machines.

ARDA AKYILDIZ received the B.S. degree in electrical engineering from Istanbul Technical University, İstanbul, Turkey, in 2022, where he is currently pursuing the M.Sc. degree in electrical engineering. His research interests include the design and optimization of wide-bandgap power devices, battery state estimation, and energy management systems.

BATI EREN ERGUN received the B.S. degree in electrical engineering from Istanbul Technical University, Turkey, in 2022, where he is currently pursuing the M.S. degree. Since beginning his role as a Research Assistant, in 2022, he has been actively involved with the Electrical Machines Laboratory, Istanbul Technical University, where he is also a Research Assistant. His research interests include the design, analysis, control, and harmonics of electrical machines, including the development of innovative generator designs for wind turbines, wide-bandgap power devices for highly efficient and compact electrical drive systems and power converters, the development of battery aging and energy management models in electric vehicles, and traction motor and inverter design.

MEHMET ONUR GULBAHCE (Member, IEEE) received the B.Sc. degree in electrical and electronics engineering from Istanbul University, İstanbul, Turkey, in 2010, and the M.Sc. degree in electrical engineering and the Ph.D. degree in electrical drives from Istanbul Technical University (ITU), İstanbul, in 2013 and 2019, respectively. During the Ph.D. degree, he was a Visiting Researcher with the Power Electronic Systems Laboratory, ETH Zürich. Between 2019 and 2021, he was an Assistant Professor with the Department of Electrical and Electronics Engineering, Fatih Sultan Mehmet Vakif University (FSMVU). He is currently an Assistant Professor with the Department of Electrical Engineering, ITU. His research interests include novel high-speed electrical machine topologies, harmonics in electrical machines and wide-bandgap power devices for very efficient and compact electrical drive systems, and power converters.